Article

Not peer-reviewed version

# Peroxymonosulfate Activation by Fe@N Co-doped BC for the Degradation of Sulfamethoxazole: The Key Role of Pyrrolic N

Tong Liu , Chen-Xuan Li * , Xing Chen , Yihan Chen , Kangping Cui * , Dejin Wang , Qiang Wei *

Posted Date: 10 September 2024

doi: 10.20944/preprints202409.0831.v1

Keywords: Biochar; Sulfate radicals; Peroxymonosulfate; Pyrrolic N

*Article*

# Peroxymonosulfate Activation by Fe@N Co-Doped BC for the Degradation of Sulfamethoxazole: The Key Role of Pyrrolic N

**Tong Liu [1,2], Chen-Xuan Li [1,2], Xing Chen [1,2], Yihan Chen [1,2], Kangping Cui [1,2,*], Dejin Wang [3] and Qiang Wei [3,4,*]**

[1] School of Resources and Environmental Engineering, Hefei University of Technology, Hefei 230009, P.R. China
[2] Key Laboratory of Nanominerals and Pollution Control of Higher Education Institutes, Hefei University of Technology, Hefei 230009, P.R. China
[3] School of Resources and Environment, Anqing Normal University, Anqing 246011, P.R. China;weiqiang07@ustc.edu.cn
[4] CAS Key Laboratory of Urban Pollutant Conversion, Department of Environmental Science and Engineering, University of Science and Technology of China, Hefei 230026, P.R. China
* Correspondence: (K.C.); wangdj@aqnu.edu.cn(Q.W.); Tel: +86-0551-62901541(K.C.); +86-0551-63492298(Q.W.)

**Abstract:** In this study, Fe, N co-doped biochar (Fe@N co-doped BC) was synthesized by carbonization-pyrolysis method and used as carbocatalysts to activate peroxymonosulfate (PMS) for sulfamethoxazole (SMX) removal. In the Fe@N co-doped BC/PMS system, the degradation rate of SMX (10.0 mg·$L^{-1}$) was 90.2% within 40 min under optimal conditions. The radical quenching experiments, and electron spin resonance (ESR) analysis suggested that sulfate radicals ($SO_4^{\bullet-}$), hydroxyl radicals (•OH) and singlet oxygen ($^1O_2$) participated in the degradation process. After the reaction, the proportion of pyrrolic N apparently decreased from 57.9% to 27.1%. Pyrrolic N served as active sites to break the inert carbon network structure and promote the generation of reactive oxygen species (ROSs). Besides, pyrrolic N showed stronger interaction with PMS and significantly reduced the activation energy required for the reaction (ΔG = 23.54 kcal/mol). The utilization potentiality of Fe@N co-doped BC was systematically evaluated in terms of its reusability, and selectivity to organics. Finally, the intermediates of SMX were also detected.

**Keywords:** biochar; sulfate radicals; peroxymonosulfate; pyrrolic N

## 1. Introduction

Sulfamethoxazole (SMX), as a common drug of sulfonamides, can efficiently treat gastroenteritis, coccidiosis, diarrhea, and other infections and diseases [1]. Due to high water solubility, and potential carcinogenicity of SMX, it would have negative impact on the ecosystem [2,3]. Since SMX was challenging to be degraded by conventional treatment processes, it was urgent to explore an efficient, low-cost, and simple technology for eliminating residual SMX in the aquatic environment.

Advanced oxidation processes (AOPs) have received huge attention due to their high efficiency and extensive adaptability [4]. Among AOPs, persulfate-based advanced oxidation processes (PS-AOPs) have gradually emerged due to its unique advantages such as higher oxidation potential and wider applicability under the environments [5,6]. As a result, there are several approaches for peroxydisulfate (PDS) and peroxymonosulfate (PMS) activation to produce reactive oxygen species (ROSs), such as electrolysis, ultrasound, ultraviolet irradiation, heat, and transition metals [7]. Among these activation methods, biochar-based catalysts have the advantages of less pollution and superior thermal stability [6].

Biochar (BC) was produced via thermochemical treatment of biomass under oxygen-limited atmosphere [8]. Biomass feedstock, such as citrus peels, maize stalk, sawdust, corncob, wood chips and shrimp shell, is rich and low-cost [9]. Furthermore, BC is featured with abundant oxygen-containing functional groups (e.g., C-OH, -COOH, C=O) and micropore or mesopore structures [10]. The redox cycle of metal ions (e.g., $Fe^{3+}/Fe^{2+}$, $Cu^{2+}/Cu^{+}$) could contribute to generating ROSs in the

 doi:10.20944/preprints202409.0831.v1



catalytic oxidation processes due to consecutive cleavage of the peroxide bond (O-O) [11]. Nitrogen doping could adjust the chemical property of the graphitic structure, increase the electron cloud density of the carbon atoms around them, thus regulate chemical properties of biochar-based catalysts [12].

Herein, Fe, N co-doped biochar (Fe@N co-doped BC) was prepared by carbonization-pyrolysis method and used as a PMS activator for the elimination of SMX. Characterizations and batch experiments were employed to assess the degradation ability of Fe@N co-doped BC. Then, the active species in the Fe@N co-doped BC/PMS system were identified by quenching tests and electron spin resonance (ESR) tests. The activation mechanism of PMS near different N configurations was uncovered by X-ray-photoelectron-spectroscopy (XPS) analysis and density functional theory (DFT) calculation. Additionally, the reusability, universal applicability, and mineralization capacity were evaluated.

## 2. Results and Discussion

### *2.1. Characterization*

Morphologies of samples were explored using scanning electron microscopy (SEM). The surface of primary BC is smooth and blocky. After the doping of urea, a layer of bright blocky stack appeared on the surface of N-doped BC (Figure 1a,b). A large number of iron oxide particles are gathered on the surface of Fe-doped BC, while the carbon substrate exhibits a regular blocky structure (Figure 1c). The surface of Fe@N co-doped BC is loaded with tiny iron oxide nanoparticles, and no isolated distribution of nanoparticles is observed outside the carbon matrix, indicating that these nanoparticles have been anchored to the carbon layer (Figure 1d).

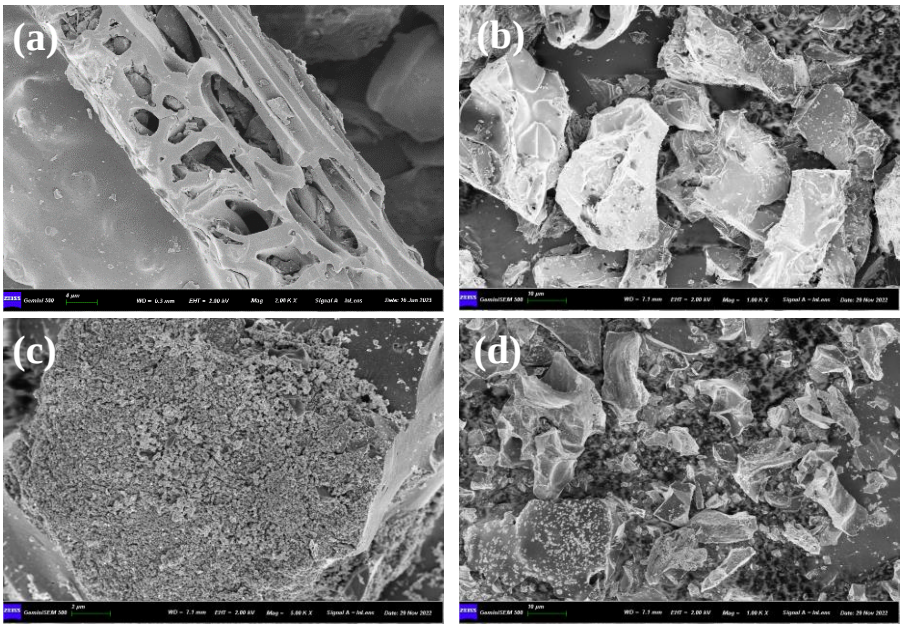


**Figure 1.** SEM images of BC (a), N-doped BC (b), Fe-doped BC (c), and Fe@N co-doped BC (d).

Besides, the ultrastructure of crystal lattice of Fe@N co-doped BC was studied in the high-resolution transmission electron microscope (HRTEM) and selected area electron diffraction (SAED) pattern. As shown in Figure 2a, iron oxide particles are successfully grown on the surface of BC by carbonization-pyrolysis method, and iron oxide particles can be used as the active site for activating PMS. The (444) crystal faces belonging to $Fe_3O_4$ with lattice spacing of 1.21 nm are calculated by Fast Fourier Transform (FFT), as depicted in Figure 2b. The Miller concentric rings also exhibit Fe@N co-doped BC crystal phase structure, and the Miller index of (111) and (311) also testifies to the formation of $Fe_3O_4$ on the surface of BC (Figure 2c). Energy dispersive spectroscopy (EDS) shows the distribution of five elements, C, Fe, Si, N and O, and also proves that iron and nitrogen have been successfully incorporated into the carbon material (Figure 2d).

Preprints.org (www.preprints.org) | NOT PEER-REVIEWED | Posted: 10 September 2024 doi:10.20944/preprints202409.0831.v1



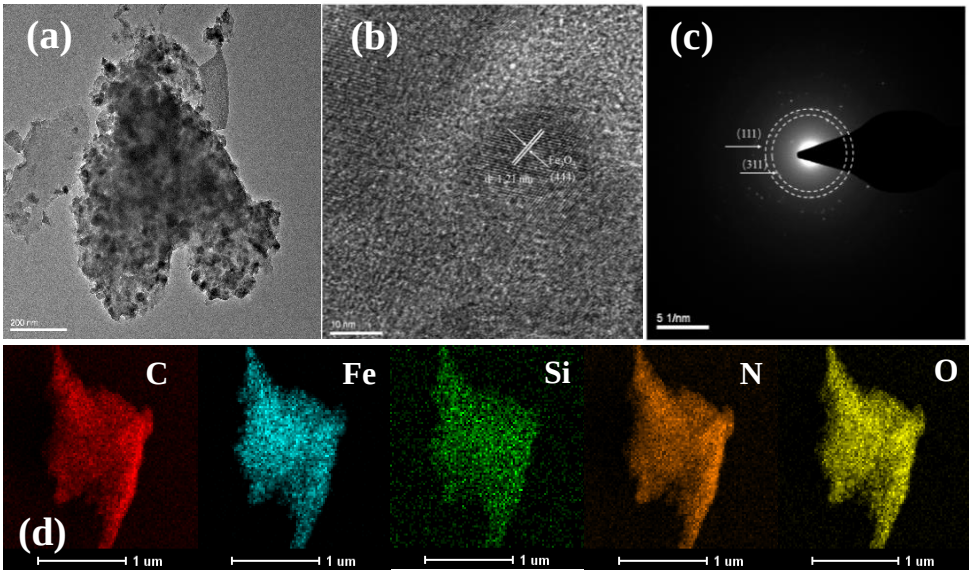


**Figure 2.** HRTEM images (a-b), SAED (c), and element distribution (d) of Fe@N co-doped BC.

XRD spectrum of samples are depicted in Figure 3a. The diffraction peaks of BC appear at about 21.6°, corresponding to the C (111) crystal plane respectively. Interestingly, N-doped BC significantly increases the diffraction peak width at 26.6°, which may be due to the incorporation of urea. It has been reported that the addition of urea can improve the graphitization degree of biochar [12]. Fe@N co-doped BC and Fe-doped BC exhibit distinct diffraction peaks at 30.1°, 35.4°, 43.1°, 53.4°, 56.9°, and 62.5°, corresponding to the crystal plane of (220), (311), (400), (422), (511), and (440), respectively. It was demonstrated that $Fe_3O_4$ nanoparticles had been successfully loaded onto biochar surfaces (JCPDS 89−2355).

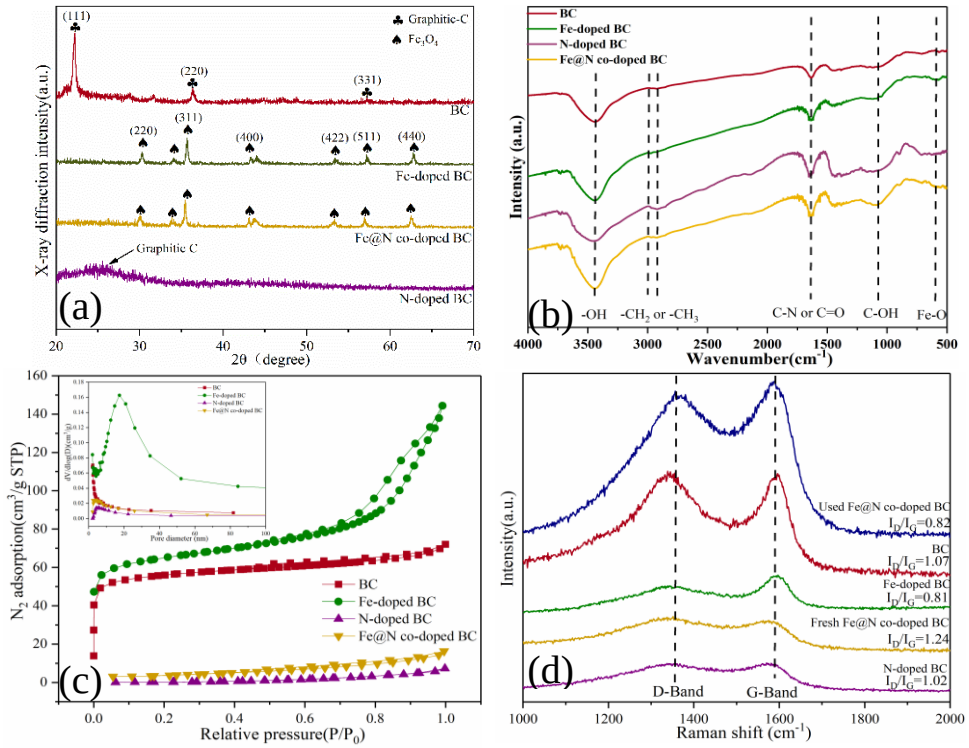


**Figure 3.** XRD patterns (a), FT-IR spectra (b), Nitrogen adsorption–desorption isotherms and pore size distribution (c) and Raman spectra (d) of catalysts.

 doi:10.20944/preprints202409.0831.v1



FT-IR spectrum exhibits the surface functional groups (Figure 3b). The peaks at 3446 $cm^{-1}$ are attributed to the stretching vibration of -OH groups [14]. The content of -OH groups on the surface of Fe@N co-doped BC is significantly higher than that on Fe-doped BC, N-doped BC and BC. The absorption peaks at 2922 $cm^{-1}$ and 2852 $cm^{-1}$ are attributed to $-CH_2$ and $-CH_3$ groups, respectively [15]. The absorption peaks at 1116 $cm^{-1}$ and 1384 $cm^{-1}$ are attributed to the vibrations of C-OH and C-C [16]. In addition, the absorption peak at 570 $cm^{-1}$ is caused by the tensile vibration of Fe-O, which also indicates that Fe and N co-doping breaks the inert structure of the carbon network and generates a new active center [17].

$N_2$ adsorption-desorption isotherms (Figure 3c) indicate the specific surface areas (SSAs) of N-doped BC (287.67 $m^2 \cdot g^{-1}$) are larger than that of BC (194.86 $m^2 \cdot g^{-1}$), Fe@N co-doped BC (269.21 $m^2 \cdot g^{-1}$) and Fe-doped BC (216.38 $m^2 \cdot g^{-1}$) (Table 1).

**Table 1.** BET and BJH results of different catalysts.

| Samples | $S_{BET}$ ($m^2/g$) [a] | Pore volume ($cm^3/g$) [a] | Average pore diameter (nm) [a] | $I_D/I_G$ [b] |
|---|---|---|---|---|
| BC | 194.86 | 0.110 | 2.46 | 1.07 |
| Fe-doped BC | 216.38 | 0.220 | 3.64 | 0.81 |
| N-doped BC | 287.67 | 0.300 | 3.56 | 1.02 |
| Fe@N co-doped BC | 269.21 | 0.240 | 3.48 | 2.14 |

[a] Obtained by Langmuir modelling studies. [b] Analyzed by Raman spectra.

As shown in Figure 3d, the appearance of both D-band and G-band of catalysts reveals the co-presence of disordered and crystalline graphite structures [18]. Furthermore, the ratio of $I_D/I_G$ is the key parameter to indicate the defective degree of catalysts [19,20]. The $I_D/I_G$ is 1.07, 0.81, 1.02, and 2.14 for BC, Fe-doped BC, N-doped BC, and Fe@N co-doped BC, respectively. The result demonstrates that Fe@N co-doped BC has obtained abundant defects (vacancy and edge defects) during pyrolysis, which is conducive to catalytic oxidation [10].

*2.2. Catalytic Oxidation of SMX*

The adsorption efficiency of different catalysts for SMX is shown in Figure 4. Under the conditions of pH = 7.0, dosage of catalyst is 0.4 g/L, and reaction temperature is 25°C, the adsorption rate of BC, Fe-doped BC, N-doped BC, and Fe@N co-doped BC for SMX is 25.8%, 23.2%, 30.0%, and 27.9%, respectively, for 40 mins. It is clear that the adsorption performance of N-doped BC is higher than that of BC, Fe-doped BC and Fe@N co-doped BC, which may be due to the doped urea, which gives a porous structure [21]. It is worth noting that neither Fe-doped BC nor Fe@N co-doped BC has a lower adsorption rate of 30.0% for SMX within 40 mins, which indicates that the iron species loaded on the carbon surface may block part of the adsorption sites, then the adsorption performance of the material is reduced.

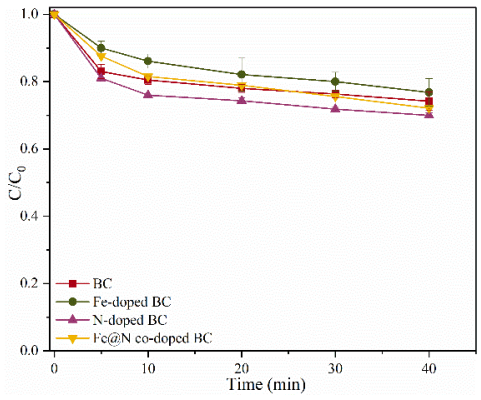

 doi:10.20944/preprints202409.0831.v1



**Figure 4.** The adsorption efficiencies of SMX in various reaction systems. Reaction conditions: $[SMX]_0$ = 10.0 mg/L, $[catalyst]_0$ = 0.4 g/L, initial pH = 7.0 and T = 25°C.

Without adding any catalyst, the degradation rate of SMX in sole PMS system is 8.0%, which indicates that the self-decomposition ability of PMS is low (Figure 5a). In the BC/PMS system, the degradation rate of SMX increased to 67.3%, indicating that BC can activate PMS to a certain extent. N and Fe doping alone can partially improve the degradation rate of BC, and the degradation rate of N-doped BC and Fe-doped BC for SMX is 69.0% and 71.0%, respectively. Fe@N co-doped BC has the highest catalytic activity under conditions of pH = 7.0, initial SMX concentration of 10.0 mg/L, Fe@N doped BC of 0.4 g/L, PMS concentration of 0.6 mM, and reaction temperature of 25°C, the degradation rate of SMX can reach 90.2%.

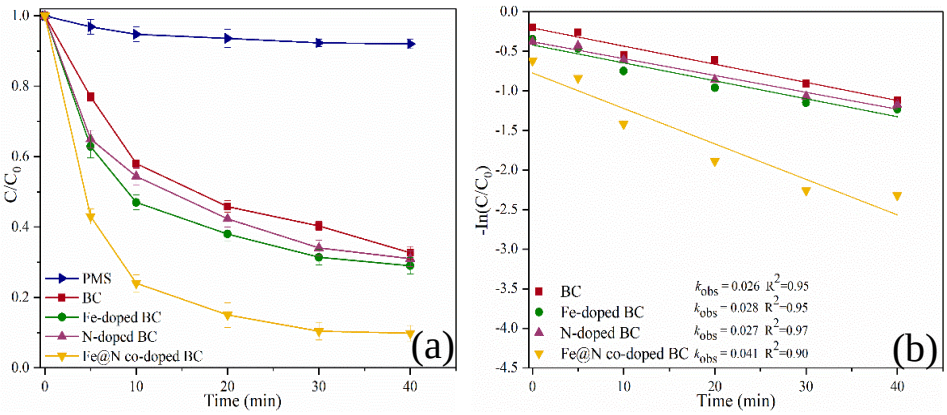


**Figure 5.** SMX degradation rates (a), and $k_{obs}$ in different systems (b). Reaction conditions: $[SMX]_0$ = 10.0 mg/L, $[catalyst]_0$ = 0.4 g/L, $[PMS]_0$ = 0.6 mM, initial pH = 7.0 and T = 25°C.

In addition, the pseudo-first-order kinetic model was used to study the degradation process of SMX in different catalytic systems (Eq. 1) (Figure 5b). The linear regression coefficients ($R^2$) were all over 0.90, indicating that the reaction kinetics of degradation of SMX by each catalyst were consistent with pseudo-first-order kinetics. The reaction rate constant ($k_{obs}$) of Fe@N co-doped BC/PMS system was 0.041 $min^{-1}$, being about 1.50, 1.40, and 1.60 times that of N-doped BC/PMS, Fe-doped BC/PMS, and BC/PMS systems, respectively (Table S1). The typical pollutants degradation rates in different systems were studied in Table S2.

$$\ln(C_t/C_0) = -kt \quad (1)$$

To explore the catalytic performance of Fe@N co-doped BC in depth, the residual PMS concentration was detected by the ABTs colorimetric method. The decomposition rate of PMS in the Fe@N co-doped BC/PMS system was 98.6% within 40 min (Figure 6). It was suggested that the favorable degradation rate of SMX in the Fe@N co-doped BC /PMS system could be due to the rapid decomposition of PMS.

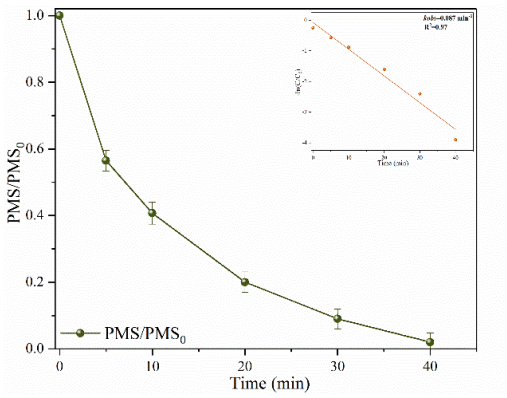

 doi:10.20944/preprints202409.0831.v1



**Figure 6.** Residual PMS in the Fe@N co-doped BC/PMS system. Reaction conditions: $[SMX]_0$ = 10.0 mg/L, $[catalyst]_0$ = 0.4 g/L, $[PMS]_0$ = 0.6 mM, initial pH = 7.0 and T = 25°C.

The effects of Fe@N co-doped BC dosage, PMS concentration, initial pH, and SMX concentration on SMX degradation were investigated (Figure 7). In the tested range, an increase of Fe@N co-doped BC dosage and PMS concentration results in an increase in the SMX degradation rate, as an increase in the Fe@N co-doped BC and PMS dosage is conducive to the rapid generation of ROSs in the Fe@N co-doped BC/PMS system [22]. The initial pH of the solution has a significant effect on the SMX removal efficiency. Under neutral conditions (pH = 7.0), the degradation rate of SMX in the Fe@N co-doped BC/PMS system is as high as 90.2%. Under the condition of strong acidity (pH = 3.0), the degradation rate of SMX decreased from 90.2% to 57.6%. Under strong alkaline conditions (pH = 11.0), the degradation rate of SMX decreased from 90.2% to 65.5%. When the initial concentrations of SMX were 0.5 mg/L, 1.0 mg/L, 5.0 mg/L and 10.0 mg/L, the degradation rates of SMX were 98.8%, 98.6%, 95.7% and 90.2%, respectively. In the test range, the initial concentration of pollutants has a slight effect on the degradation rate of SMX.

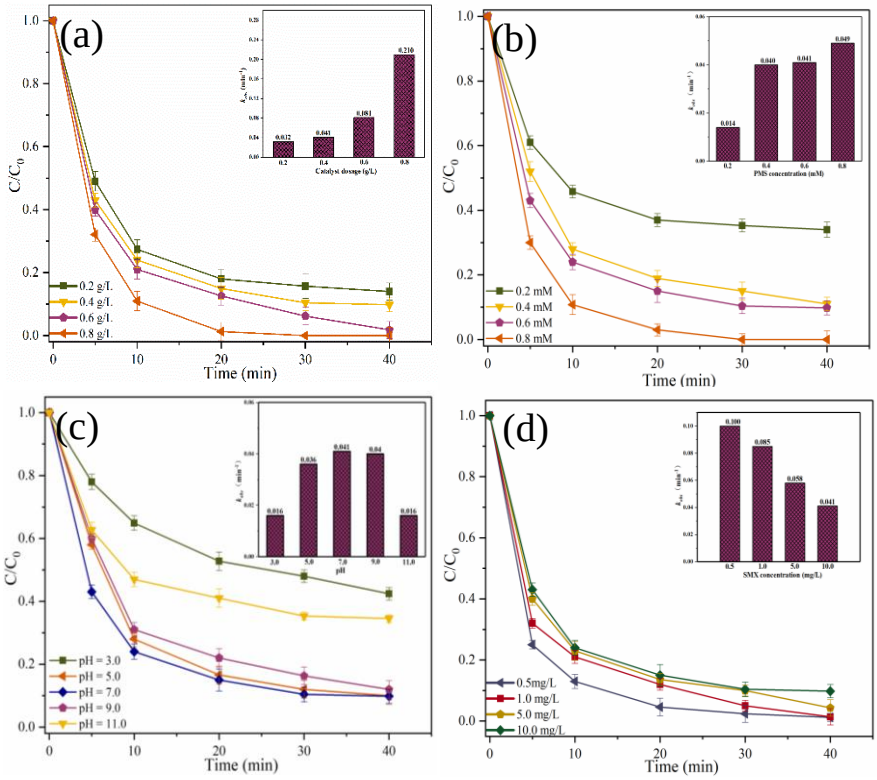


**Figure 7.** Effects of different parameters on SMX removal in Fe@N co-doped BC/PMS system: (a) catalyst dosage, (b) PMS concentration, (c) solution pH, (d) SMX concentration. (Conditions: pH = 7.0; $[SMX]_0$ = 10.0 mg/L; [catalyst] = 0.4 g/L; [PMS] = 0.6 mM; T = 25°C).

Co-existing ions can restrain the SMX removal by interacting with reactive species [23]. Typical anions ($Cl^-$, $H_2PO_4^-$, $HCO_3^-$), and humic acid (HA) restrained the SMX elimination to varying degrees (Figure S1). When 5.0 mM and 500.0 mM $Cl^-$ were present in the Fe@N co-doped BC/PMS system, SMX removal rate decreased from 90.2% to 79.0% and 70.0%, respectively, within 40 min. The corresponding $k_{obs}$ decreased from 0.041 $min^{-1}$ to 0.025 $min^{-1}$ and 0.021 $min^{-1}$, which was mainly due to the formation of active chlorine species [24,25]. Compared with $Cl^-$, $HCO_3^-$ and $H_2PO_4^-$ have a more significant inhibitory effect on SMX degradation due to the fact that $HCO_3^-$ reacts with •OH and $SO_4^{\bullet-}$ to form $CO_3^{\bullet-}$ which has a lower redox potential [26]. Similarly, $H_2PO_4^-$ reacts with $SO_4^{\bullet-}$ to produce less active free radicals, thereby reducing the degradation rate of SMX. In addition, $H_2PO_4^-$ easily binds to the active sites on the surface of Fe@N co-doped BC, preventing the catalyst from producing

 doi:10.20944/preprints202409.0831.v1



enough ROSs to degrade SMX [27]. When 20.0 mg/L and 50.0 mg/L HA were present in the reaction system, the degradation rates of SMX decreased from 90.2% to 81.0% and 62.0%, respectively, and the corresponding $k_{obs}$ decreased from 0.041 $min^{-1}$ to 0.033 $min^{-1}$ and 0.019 $min^{-1}$, respectively, within 40 min. On the one hand, HA can consume •OH and $SO_4^{\bullet-}$; on the other hand, HA has a strong π-π superposition effect, which is easy to deposit on the surface of Fe@N co-doped BC, thus inhibiting the interaction between Fe@N co-doped BC, PMS and SMX [28].

Figure S2a exhibited the degradation rates of various pharmaceuticals and personal care products (PPCPs) in Fe@N co-doped BC/PMS system. The degradation efficiencies of tetracycline hydrochloride (TC), 4-chloro-3-methyl phenol (CMP), norfloxacin (NOR), and acetaminophen (ACT) were 95.8%, 93.3%, 91.5%, and 94.2% respectively in 40 min. In general, representative PPCPs could be removed efficiently in Fe@N co-doped BC/PMS system. To study the reusability of Fe@N co-doped BC, 5 consecutive degradation tests were conducted (Figure S2(b)). After 5 cycles, the degradation rate of SMX within 40 min decreased from 90.2% to 63.0%. This could be due to the sedimentation of intermediates on the surface of Fe@N co-doped BC, which occupied the reactive sites for activating PMS. The saturation magnetization value of Fe@N co-doped BC was 17.43 emu/g (Figure S2(c)). Fe@N co-doped BC exhibited a strong magnetic response to an external magnetic field and is easily separated from the SMX solution, facilitating the recycling of the catalyst. Figure S2(d) displayed the continuous leaching of Fe species in the redox process. Fortunately, less than 1.04 mg/L of Fe species were leached in reaction solution.

### *2.3. Mechanism Discussion*

#### 2.3.1. Identification of ROSs

The above results indicate that SMX can be degraded rapidly in the Fe@N co-doped BC/PMS system, while previous studies have shown that SMX may be degraded via either a radical pathway ($O_2^{\bullet-}$, •OH, or $SO_4^{\bullet-}$) or a non-radical pathway ($^1O_2$ or biochar-PMS* complex) in a heterogeneous catalytic oxidation system [6]. To determine the active species produced in this system and their contribution to SMX degradation, quenching experiments and ESR tests were performed. •OH, •OH/$SO_4^{\bullet-}$ and $O_2^{\bullet-}$ were quenched by *Tert*-butanol (TBA), methanol (MeOH) and *p*-benzoquinone (*p*-BQ), respectively, while furfuryl alcohol (FFA) and *L*-histidine (*L*-his) were used as trapping agents for $^1O_2$ [29,30]. The SMX removal rates decreased from 92.0% to 33.4%, 73.5%, 86.7%, 73.2% and 71.8% within 40 min after adding MeOH (0.5 M), TBA (0.5 M), *p*-BQ (0.1 M), *L*-his (0.1 M) and FFA (0.1 M), respectively (Figure 8). These results indicate that •OH and $SO_4^{\bullet-}$ exist in the system, and $SO_4^{\bullet-}$ may play a dominant role. Since *p*-BQ has a slight inhibitory effect on SMX degradation, the system does not produce large amounts of $O_2^{\bullet-}$. The contribution of each reactive species was listed in Table S3.

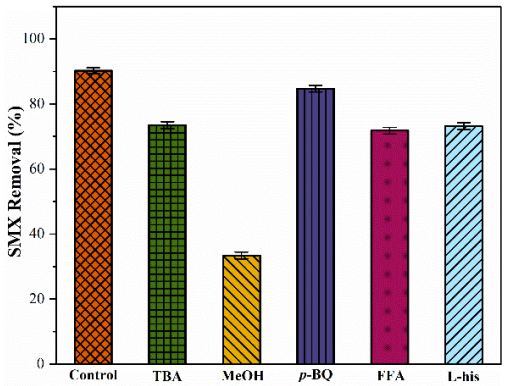


**Figure 8.** Quenching tests of the reactive species. (Conditions: pH = 7.0; $[SMX]_0$ = 10.0 mg/L; [catalyst] = 0.4 g/L; [PMS] = 0.6 mM; T = 25°C; [MeOH] = [TBA] = 500.0 mM; [FFA] = [*L*-his] = [*p*-BQ] = 100.0 mM).

ESR was performed to further prove the presence of ROSs in the Fe@N co-doped BC/PMS system using 2,2,6,6-tetramethyl-4-piperidinol (TEMP) and 5,5-dimethyl-1-pyrroline N-oxide (DMPO) as spin-trapping agents [31,32]. A spectrum with seven main peaks belonging to DMPO-X was observed

 doi:10.20944/preprints202409.0831.v1



in the Fe@N co-doped BC/PMS system, indicating that Fe@N co-doped BC activated PMS to produce •OH and $SO_4^{\bullet-}$ (Figure 9a). The signal intensity in the Fe@N co-doped BC/PMS system was significantly higher than that of the Fe-doped/PMS and N-doped/PMS system, indicating that there is a synergistic effect between Fe and N on the surface of biochar. When Fe@N co-doped BC, PMS and TEMP were added to the solution, a typical triplet signal with the intensity ratio of 1: 1: 1 verified the existence of $^1O_2$ (Figure 9b). The self-decomposition of PMS could produce a small amount of $^1O_2$ [33] . In summary, •OH, $SO_4^{\bullet-}$ and $^1O_2$ are produced in this system, in which $SO_4^{\bullet-}$ is the main active species and leads the degradation process of free radical pathway, while $^1O_2$ leads the degradation process of non-free radical pathway.

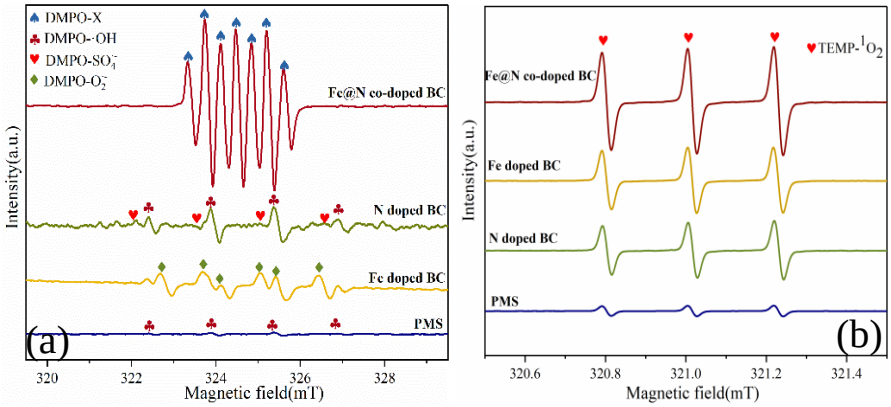


**Figure 9.** ESR spectra of (a) DMPO-X, and (b) TEMP-$^1O_2$. (Conditions: $[SMX]_0$ = 10.0 mg/L; $[Catalyst]_0$ = 0.4 g/L; $[PMS]_0$ = 0.6 mM; pH = 7.0; T = 25°C; [TEMP] = [DMPO] = 10.0 mM).

### 2.3.2. Reaction Mechanism

The above experiments demonstrate the production of •OH, $SO_4^{\bullet-}$ and $^1O_2$ in the Fe@N co-doped BC/PMS system, and on the basis of this, the general catalytic mechanism is proposed. First, •OH and $SO_4^{\bullet-}$ may be produced by the destruction of the O-O bond of the PMS by free-flowing π electrons on the $sp^2$ hybrid carbon (Eqs. (1–3)). As can be seen from the XPS spectrum (Figure 10a), the surface of Fe@N co-doped BC is successfully doped with iron and nitrogen, and the specific atomic percentages of the obtained catalyst are shown in Table S4. Fe@N co-doped BC surface contains C-OH, COOH and C=O groups, which can serve as an active site (Figure 10b). As an electron donor functional group, C-OH is more inclined to activate PMS to produce free radicals, such as •OH and $SO_4^{\bullet-}$. As electron withdrawing functional groups, C=O and COOH are more inclined to degrade SMX through non-radical pathway. After the catalytic reaction, Fe (II) content decreased from 43.7% to 40.8%, while Fe (III) content increased from 36.4% to 37.9% (Figure 10c). The doped Fe (II) reacts with $HSO_5^-$ to form •OH and $SO_4^{\bullet-}$ (Eqs. (4–5)), and the generated free radicals can be converted flexibly. Subsequently, Fe (III) reacts with $HSO_5^-$ to produce $SO_5^{\bullet-}$, and Fe (III) is reduced to Fe (II) and maintains a complete cycle (Eq. 6). These results indicate that $Fe_3O_4$ plays a leading role in the activation of PMS in the free radical pathway.

 doi:10.20944/preprints202409.0831.v1



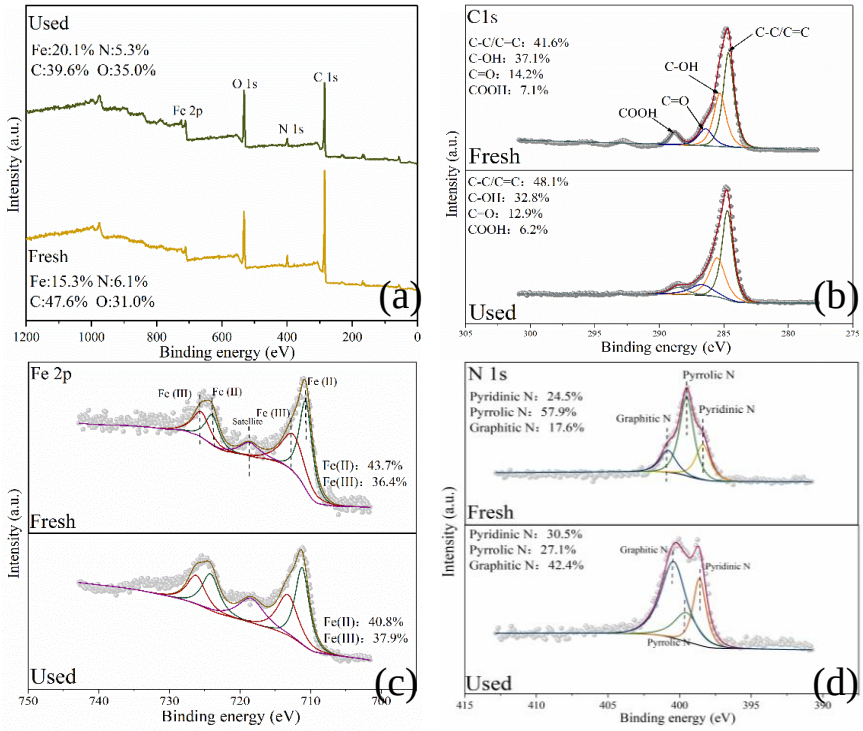


**Figure 10.** XPS spectra of full-range survey (a), C 1s (b), Fe 2p (c), N 1s (d) for Fe@N co-doped BC.

It has been reported that carbon-based materials can also activate PMS to degrade organic micropollutants through non-free radical pathways, and the non-free radical mechanism may be related to nitrogen doping [34,35]. N 1s can be divided into three peaks, including pyrrolic N, pyridinic N and graphitic N (Figure 10d). The content of graphitic N and pyridinic N increased from 17.6% and 24.5% to 42.4% and 30.5% respectively, while the content of pyrrolic N decreased from 57.9% to 27.1%. Therefore, pyrrolic N is considered to be the main active species in the redox process.

$$\pi - \text{electrons} + HSO_5^- \rightarrow SO_4^{\cdot -} + OH^- \quad (1)$$

$$\pi - \text{electrons} + HSO_5^- \rightarrow \cdot OH + SO_4^{2-} \quad (2)$$

$$SO_4^{\cdot -} + H_2O \rightarrow H^+ + SO_4^{2-} + \cdot OH \quad (3)$$

$$Fe^{2+} + HSO_5^- \rightarrow Fe^{3+} + SO_4^{\cdot -} + OH^- \quad (4)$$

$$Fe^{2+} + HSO_5^- \rightarrow Fe^{3+} + SO_4^{2-} + \cdot OH \quad (5)$$

$$Fe^{3+} + HSO_5^- \rightarrow Fe^{2+} + SO_5^{\cdot -} + H^+ \quad (6)$$

The PMS activation performances of three N configurations, pyrrolic N, pyridinic N and graphitic N, were compared, as shown in Figure 11. From the top view, it can be seen that PMS can be stably adsorbed on top of pyrrolic N, pyridinic N and graphitic N. For the reactant structure, the distance (D) between PMS and pyrrolic N is the shortest (2.986 Å). The transition state energy barrier of pyrrolic N/PMS, pyridinic N/PMS and graphitic N/PMS was calculated by B3LYP/6-31G (d,p) method as 23.54 kcal/mol, 27.81 kcal/mol and 26.45 kcal/mol, respectively. The above results showed that pyrrolic N could significantly reduce the activation energy required for the reaction, and the catalytic activity of this active site was the highest.

Preprints.org (www.preprints.org) | NOT PEER-REVIEWED | Posted: 10 September 2024 doi:10.20944/preprints202409.0831.v1



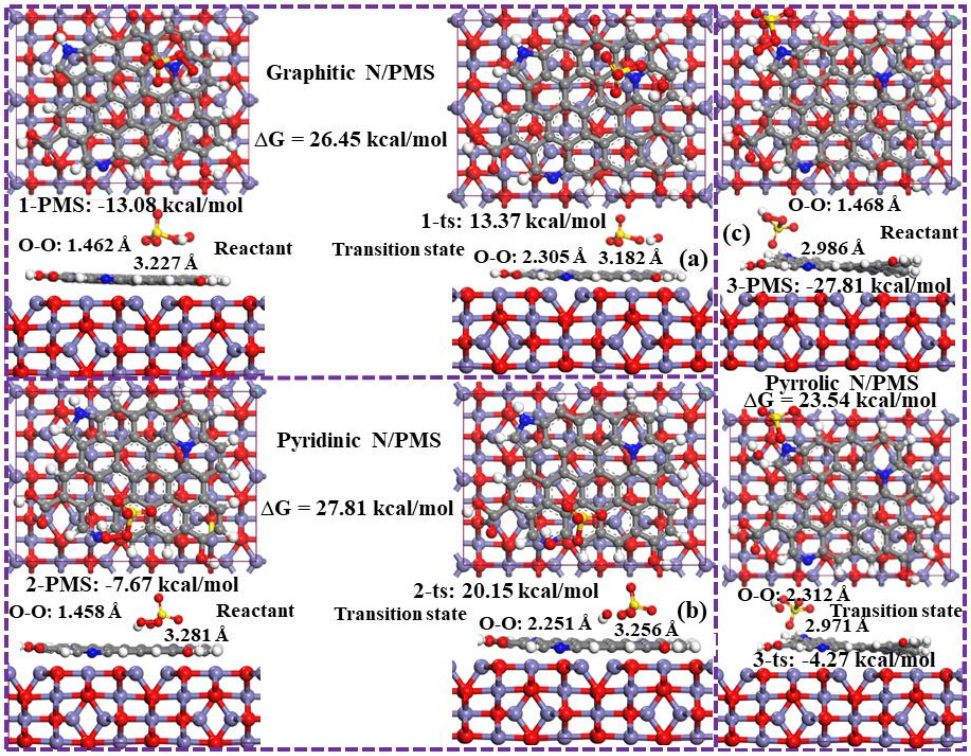


**Figure 11.** The optimization structures of PMS adsorption on different N substitution sites and the corresponding transition state. (a) Graphitic N/PMS, (b) pyridinic N/PMS, and (c) pyrrolic N/PMS.

To investigate the charge transfer rate on the surface of carbon-based materials, electrochemical tests were carried out. Electrochemical impedance spectroscopy (EIS) shows that Fe@N co-doped BC has a smaller semicircle diameter and therefore lower electron migration resistance than that of BC, Fe-doped BC, and N-doped BC (Figure 12). The hydrophilicity of carbon-based materials was further investigated by measuring the contact angle [21] (Figure 13). The contact angle of Fe@N co-doped BC is 4.7°, which is lower than that of BC (14.8°), N-doped BC (9.0°), and Fe-doped BC (9.3°), which means that Fe@N co-doped BC has higher hydrophilicity and is easier to obtain excellent degradation properties.

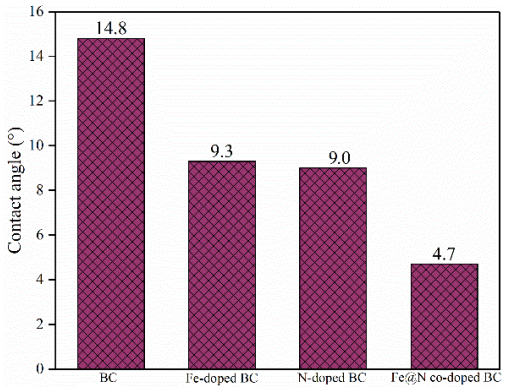


**Figure 12.** EIS Nyquist plots of various carbon-based catalysts.

Preprints.org (www.preprints.org) | NOT PEER-REVIEWED | Posted: 10 September 2024 doi:10.20944/preprints202409.0831.v1



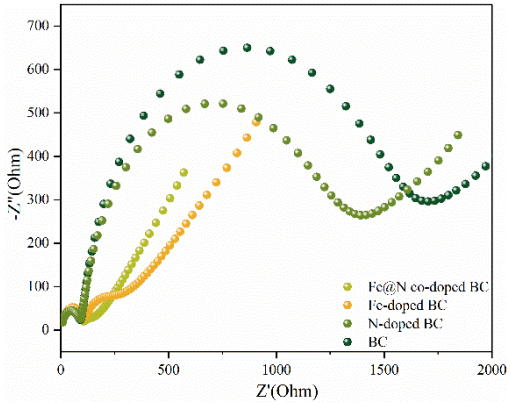


**Figure 13.** The contact angle of catalysts.

*2.4. Degradation Pathways of SMX*

The intermediate products of SMX degradation were investigated by UPLC-TOF/MS (Figure S3, Figure S4 and Table S5). In pathway I, the C atom on the isoxazole ring of SMX undergoes electrophilic addition reaction to produce the product I (m/z = 288) [1]. Subsequently, the S-N bond of SMX breaks and product I is transformed into product II (m/z = 133) and product III (m/z = 190). Under ROSs's attack, the N-O bond on the isoxazole ring breaks to produce product IV (m/z = 117), which is eventually mineralized into $CO_2$ and $H_2O$. At the same time, a ring-opening reaction may occur on the isoxazole ring of product I to form product VI (m/z = 246), and a subsequent dehydrogenation reaction to form intermediate product VII (m/z = 216). In pathway III, SMX undergoes electrophilic substitution to produce a product IX (m/z = 270). Subsequently, the S-N bond of SMX breaks and product IX is transformed into product X (m/z = 190) and product XI (m/z = 99). Under ROSs's attack, product XI was further oxidized to product XII and product XIII. In summary, the degradation mechanism of SMX in the Fe@N co-doped BC/PMS system is shown in Figure 14.

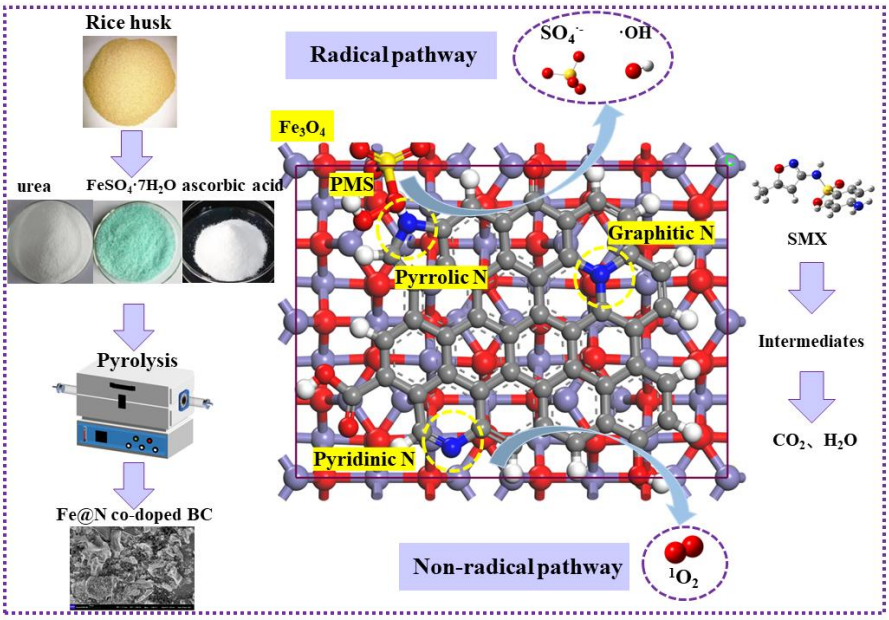


**Figure 14.** Proposed mechanism of SMX degradation in Fe@N co-doped BC/PMS system.

## 3. Materials and Methods

*3.1. Preparation of Catalysts*

Slow pyrolysis, as a typical carbonization method, was commonly used for the conversion of biomass wastes into biochar with high carbon and low volatile matter contents [13]. In this work, Fe@N co-doped BC was fabricated using carbonization-pyrolysis strategy [12]. Rice husk was

 doi:10.20944/preprints202409.0831.v1



purchased from a biomass pyrolysis power plant in China. Firstly, biomass was washed, dried in a vacuum drying oven at 100°C for 12 h, ground, and then passed through a 100-mesh sieve to acquire thin powders for further use. 5.56 g $FeSO_4 \cdot 7H_2O$, 3.00 g urea and 2.50 g ascorbic acid was dissolved into 100 mL deionized water, after that 3.00 g powders were added into the solution and adequately shaken in thermostatic shaking bath. The mixture was dried in a vacuum drying oven for 24 h, and calcined at a constant calcination temperature (800°C) under $N_2$ atmosphere (5°C/min. of heating rate) for 2 h. The catalyst was washed with deionized water for several times, and the resulting composites were denoted as Fe@N co-doped BC. For comparison, Fe-doped BC, N-doped BC and BC were synthesized in the same method.

### *3.2. Reaction Procedures*

Batch experiments were carried out in 50 mL vials containing 50 mL of SMX (10 mg/L) to evaluate the catalytic ability of Fe@N co-doped BC on PMS activation. The range of Fe@N co-doped BC dosing was 0.2−0.8 g/L, the concentration of PMS was 0.2−0.8 mM, the pH was 3.0−11.0, SMX concentration was 0.5−10.0 mg/L, and the reaction temperature was set to 25°C. All experiments were carried out at 150 rpm, and 1.0 mL reaction solution was taken periodically at intervals and filtered through a 0.22 μm filter. The excess reaction was terminated by adding 1 mL $Na_2S_2O_3$ (0.2 M). 0.1 M NaOH or $H_2SO_4$ was added into the reaction solution to adjust the initial pH values before reaction. All experiments were performed in triplicate.

## 4. Conclusions

In summary, Fe@N co-doped BC was prepared by carbonization-pyrolysis method, and the catalyst obtained abundant catalytic centers ($Fe_3O_4$, pyrrolic N) and defect sites ($I_D/I_G$ = 0.97). Under optimal conditions, the degradation rate of SMX in the Fe@N co-doped BC/PMS system is 90.2%. The degradation process conforms to pseudo-first-order kinetics with a $k_{obs}$ of 0.041 $min^{-1}$. In addition, various typical PPCPs could be efficiently degraded in the Fe@N co-doped BC/PMS system within 40 mins. The quenching experiment and ESR test results show that •OH, $SO_4^{\bullet-}$ and $^1O_2$ were produced in the Fe@N co-doped BC/PMS system, in which $SO_4^{\bullet-}$ is the main active species. $SO_4^{\bullet-}$ can be produced in the redox cycle between Fe (III) and Fe (II), and $Fe_3O_4$ acts as an important catalytic center to break the inert carbon network structure and promote the formation of ROSs in the reaction system. Before and after the reaction, the content of pyrrolic N decreased from 57.9% to 27.1%. As the main active site, pyrrolic N showed stronger interaction with PMS and significantly reduced the activation energy required for the reaction ($\Delta G$ = 23.54 kcal/mol). Therefore, this work first solves the problem of low catalytic activity caused by the lack of catalytic center of carbon materials. In addition, the strong magnetic Fe@N co-doped BC has good recyclability, which improves the practical application and long-term operational potential of the system.

**Declaration of Competing Interest:** The authors declare no competing interests.

**Acknowledgments:** The work was supported by National Key R&D Program of China (2019YFC0408500), Major Science and Technology Projects of Anhui Province (201903a07020009, 202003a07020004), Hefei independent innovation policy loan transfer subsidy project (J2020K07), the National Natural Science Foundation of China (52300016), China Postdoctoral Science Foun-dation (No. 2023M733379).

## References

1. J. Du, W. Guo, H. Wang, R. Yin, H. Zheng, X. Feng, D. Che, N. Ren, Hydroxyl radical dominated degradation of aquatic sulfamethoxazole by Fe(0)/bisulfite/O2: Kinetics, mechanisms, and pathways, Water Res, 138 (2018) 323-332.
2. M. Xu, J. Li, Y. Yan, X. Zhao, J. Yan, Y. Zhang, B. Lai, X. Chen, L. Song, Catalytic degradation of sulfamethoxazole through peroxymonosulfate activated with expanded graphite loaded CoFe2O4 particles, Chemical Engineering Journal, 369 (2019) 403-413.
3. Y. Xu, S. Liu, M. Wang, J. Zhang, H. Ding, Y. Song, Y. Zhu, Q. Pan, C. Zhao, H. Deng, Thiourea-assisted one-step fabrication of a novel nitrogen and sulfur co-doped biochar from nanocellulose as metal-free catalyst for efficient activation of peroxymonosulfate, J Hazard Mater, 416 (2021) 125796.

4. L. Xu, B. Fu, Y. Sun, P. Jin, X. Bai, X. Jin, X. Shi, Y. Wang, S. Nie, Degradation of organic pollutants by Fe/N co-doped biochar via peroxymonosulfate activation: Synthesis, performance, mechanism and its potential for practical application, Chemical Engineering Journal, 400 (2020).
5. J. Wang, S. Wang, Activation of persulfate (PS) and peroxymonosulfate (PMS) and application for the degradation of emerging contaminants, Chemical Engineering Journal, 334 (2018) 1502-1517.
6. C. Zhao, B. Shao, M. Yan, Z. Liu, Q. Liang, Q. He, T. Wu, Y. Liu, Y. Pan, J. Huang, J. Wang, J. Liang, L. Tang, Activation of peroxymonosulfate by biochar-based catalysts and applications in the degradation of organic contaminants: A review, Chemical Engineering Journal, 416 (2021).
7. J. Zhen, S. Zhang, X. Zhuang, S. Ahmad, T. Lee, H. Si, C. Cao, S.-Q. Ni, Sulfate radicals based heterogeneous peroxymonosulfate system catalyzed by CuO-Fe3O4-Biochar nanocomposite for bisphenol A degradation, Journal of Water Process Engineering, 41 (2021).
8. C. Wang, R. Huang, R. Sun, J. Yang, M. Sillanpää, A review on persulfates activation by functional biochar for organic contaminants removal: Synthesis, characterizations, radical determination, and mechanism, Journal of Environmental Chemical Engineering, 9 (2021).
9. T. Liu, K. Cui, C.X. Li, Y. Chen, Q. Wang, X. Yuan, Y. Chen, J. Liu, Q. Zhang, Efficient peroxymonosulfate activation by biochar-based nanohybrids for the degradation of pharmaceutical and personal care products in aquatic environments, Chemosphere, 311 (2023) 137084.
10. J. Yu, H. Feng, L. Tang, Y. Pang, G. Zeng, Y. Lu, H. Dong, J. Wang, Y. Liu, C. Feng, J. Wang, B. Peng, S. Ye, Metal-free carbon materials for persulfate-based advanced oxidation process: Microstructure, property and tailoring, Progress in Materials Science, 111 (2020).
11. Y. Zhao, M. Song, Q. Cao, P. Sun, Y. Chen, F. Meng, The superoxide radicals' production via persulfate activated with CuFe2O4@Biochar composites to promote the redox pairs cycling for efficient degradation of o-nitrochlorobenzene in soil, J Hazard Mater, 400 (2020) 122887.
12. M. Xi, K. Cui, M. Cui, Y. Ding, Z. Guo, Y. Chen, C. Li, X. Li, Enhanced norfloxacin degradation by iron and nitrogen co-doped biochar: Revealing the radical and nonradical co-dominant mechanism of persulfate activation, Chemical Engineering Journal, 420 (2021).
13. A.A. Azzaz, C. Matei Ghimbeu, S. Jellai, L. El-Bassi, M. Jeguirim, Olive Mill by-Products Thermochemical Conversion via Hydrothermal Carbonization and Slow Pyrolysis: Detailed Comparison between the Generated Hydrochars and Biochars Characteristics, Processes, 10 (2022).
14. S. Wang, J. Wang, Activation of peroxymonosulfate by sludge-derived biochar for the degradation of triclosan in water and wastewater, Chemical Engineering Journal, 356 (2019) 350-358.
15. L. Zhao, X. Cao, O. Masek, A. Zimmerman, Heterogeneity of biochar properties as a function of feedstock sources and production temperatures, J Hazard Mater, 256-257 (2013) 1-9.
16. K. Zhu, Q. Bin, Y. Shen, J. Huang, D. He, W. Chen, In-situ formed N-doped bamboo-like carbon nanotubes encapsulated with Fe nanoparticles supported by biochar as highly efficient catalyst for activation of persulfate (PS) toward degradation of organic pollutants, Chemical Engineering Journal, 402 (2020).
17. J. Shi, Y. Wang, W. Du, Z. Hou, Synthesis of graphene encapsulated Fe3C in carbon nanotubes from biomass and its catalysis application, Carbon, 99 (2016) 330-337.
18. D.-G. Kim, S.-O. Ko, Effects of thermal modification of a biochar on persulfate activation and mechanisms of catalytic degradation of a pharmaceutical, Chemical Engineering Journal, 399 (2020).
19. J. He, Y. Xiao, J. Tang, H. Chen, H. Sun, Persulfate activation with sawdust biochar in aqueous solution by enhanced electron donor-transfer effect, Sci Total Environ, 690 (2019) 768-777.
20. Y. Shang, C. Chen, P. Zhang, Q. Yue, Y. Li, B. Gao, X. Xu, Removal of sulfamethoxazole from water via activation of persulfate by Fe3C@NCNTs including mechanism of radical and nonradical process, Chemical Engineering Journal, 375 (2019).
21. X. Li, Y. Jia, M. Zhou, X. Su, J. Sun, High-efficiency degradation of organic pollutants with Fe, N co-doped biochar catalysts via persulfate activation, J Hazard Mater, 397 (2020) 122764.
22. B. Yao, Z. Luo, S. Du, J. Yang, D. Zhi, Y. Zhou, Magnetic MgFe(2)O(4)/biochar derived from pomelo peel as a persulfate activator for levofloxacin degradation: Effects and mechanistic consideration, Bioresour Technol, 346 (2022) 126547.
23. K. Xiao, F. Liang, J. Liang, W. Xu, Z. Liu, B. Chen, X. Jiang, X. Wu, J. Xu, J. Beiyuan, H. Wang, Magnetic bimetallic Fe, Ce-embedded N-enriched porous biochar for peroxymonosulfate activation in metronidazole degradation: Applications, mechanism insight and toxicity evaluation, Chemical Engineering Journal, 433 (2022).
24. Y. Hu, D. Chen, R. Zhang, Y. Ding, Z. Ren, M. Fu, X. Cao, G. Zeng, Singlet oxygen-dominated activation of peroxymonosulfate by passion fruit shell derived biochar for catalytic degradation of tetracycline through a non-radical oxidation pathway, J Hazard Mater, 419 (2021) 126495.
25. M. Wang, H. Xu, Q. Li, G. Zhou, Q. Ye, Q. Wang, J. Zhang, Panda manure biochar-based green catalyst to remove organic pollutants by activating peroxymonosulfate: Important role of non-free radical pathways, Journal of Environmental Chemical Engineering, 9 (2021).

 doi:10.20944/preprints202409.0831.v1




26. J. Huang, Y. Cao, B. Qin, G. Zhong, J. Zhang, H. Yu, H. Wang, F. Peng, Highly efficient and acid-corrosion resistant nitrogen doped magnetic carbon nanotubes for the hexavalent chromium removal with subsequent reutilization, Chemical Engineering Journal, 361 (2019) 547-558.
27. Y. Gao, Y. Chen, T. Song, R. Su, J. Luo, Activated peroxymonosulfate with ferric chloride-modified biochar to degrade bisphenol A: Characteristics, influencing factors, reaction mechanism and reuse performance, Separation and Purification Technology, 300 (2022).
28. M. Xiong, J. Yan, G. Fan, Y. Liu, B. Chai, C. Wang, G. Song, Built-in electric field mediated peroxymonosulfate activation over biochar supported-Co3O4 catalyst for tetracycline hydrochloride degradation, Chemical Engineering Journal, 444 (2022).
29. H. Zhang, Y. Song, L.-c. Nengzi, J. Gou, B. Li, X. Cheng, Activation of persulfate by a novel magnetic CuFe2O4/Bi2O3 composite for lomefloxacin degradation, Chemical Engineering Journal, 379 (2020).
30. R. Luo, M. Li, C. Wang, M. Zhang, M.A. Nasir Khan, X. Sun, J. Shen, W. Han, L. Wang, J. Li, Singlet oxygen-dominated non-radical oxidation process for efficient degradation of bisphenol A under high salinity condition, Water Res, 148 (2019) 416-424.
31. X. Li, Z. Yang, G. Wu, Y. Huang, Z. Zheng, H.F. Garces, K. Yan, Fabrication of ultrathin lily-like NiCo2O4 nanosheets via mooring NiCo bimetallic oxide on waste biomass-derived carbon for highly efficient removal of phenolic pollutants, Chemical Engineering Journal, 441 (2022).
32. X. Huang, Z. Yu, Y. Shi, Q. Liu, S. Fang, Highly efficient activation of peroxymonosulfate by Co, S co-doped bamboo biochar for sulfamethoxazole degradation: Insights into the role of S, Journal of Environmental Chemical Engineering, 10 (2022).
33. T. Liu, K. Cui, Y. Chen, C. Li, M. Cui, H. Yao, Y. Chen, S. Wang, Removal of chlorophenols in the aquatic environment by activation of peroxymonosulfate with nMnOx@Biochar hybrid composites: Performance and mechanism, Chemosphere, 283 (2021) 131188.
34. W. Ren, G. Nie, P. Zhou, H. Zhang, X. Duan, S. Wang, The Intrinsic Nature of Persulfate Activation and N-Doping in Carbocatalysis, Environ Sci Technol, 54 (2020) 6438-6447.
35. Y. Ding, X. Wang, L. Fu, X. Peng, C. Pan, Q. Mao, C. Wang, J. Yan, Nonradicals induced degradation of organic pollutants by peroxydisulfate (PDS) and peroxymonosulfate (PMS): Recent advances and perspective, Sci Total Environ, 765 (2021) 142794.